

Evaluation of biomass and its thermal decomposition products as fuels for direct carbon fuel cells

Pradyut Kumar Swain¹ and Asit Ku Parida²

¹Aryan Institute of Engineering & Technology, Bhubaneswar, Odisha

²NM Institute of Engineering and Technology, Bhubaneswar, Odisha

ARTICLE INFO

Keywords:

Direct carbon fuel cell
Biomass
Thermal decomposition
Solid oxide fuel cell
Electrochemical performance
Degradation mechanism

ABSTRACT

The objective of this paper is to find the relationship of electrochemical performance between biomass and its thermal decomposition products, their degradation mechanisms during durability tests in solid oxide fuel cells. The properties of biomass and biochar, the electrochemical behaviours of biomass, biochar and biogas were characterized comprehensively, and subsequently the degradation process of biomass, biochar and biogas fuelled cells were analysed. It showed that raw biomass fuelled cells produced considerable peak power density (PPD, 0.144 W cm⁻² at 1123 K) but experienced rapid discharge degradation. Torrefaction pre-treatment (573K) of raw samples compromised PPDs while pyrolysis pre-treatment (973K) enhanced PPDs. With biochar as fuel, the power was generated from CO electro-oxidation and biochar-CO₂ gasification. Feeding of CO₂ into the anode chamber continuously did not improve the output performance. The degradation was mainly caused by the gradually decreasing gasification reactivity of biochar with CO₂ and slight anode carbon deposition. With the help of biogas as fuel, the anode reactions were electro-oxidation of active species like H₂, CO, CH₄, and finally the cell degraded takes place.

1. Introduction

Direct carbon fuel cell (DCFC) is an electrochemical device, which can convert the chemical energy of carbon fuels to electricity through electrochemical reactions. For the advantages of high theoretical efficiency, fuel flexibility and easy CO₂ capture, DCFC possesses a promising future to generate electricity with carbon fuels consumption [1-4]. Theoretically, fuels, including graphite, carbon black, oil coke, coal and biomass can be converted electrochemically in DCFC [5]. Among them, biomass has the characteristics of renewability, net zero carbon dioxide emission, generally low sulfur and ash content, which makes biomass a more suitable fuel in DCFC.

Unlike pure carbon fuels such as carbon black and graphite, biomass is composed of fixed carbon, moisture, volatile matter and ash based on the proximate analysis. What matters most are the effects of volatile matter and ash on the conversion of biomass in DCFCs. The content of volatile matter in traditional agroforestry biomass can be as high as 60-80%. At the temperature higher than 673 K, the volatile matter is

released, forming fixed carbon (biochar) and pyrolysis gases (biogas) [6,7]. From this point of view, the conversion process of raw biomass in DCFC is complicated as it contains the thermal decomposition of raw biomass and the electrochemical conversion of the decomposition products (biochar and biogas). The effective and stable conversion is difficult to realize as both biochar and biogas has the capability of participating in the anode reactions and at the same time causing cell degradation [8-10]. Removing volatiles through pyrolysis and using biochar as the fuel of DCFC is a potential solution, however biomass pyrolysis is energy-consuming process and the char yield is as low as 10-30%.

Both biomass with little pretreatment and biochar prepared by pyrolyzing raw biomass at 673-1173 K have been intensively investigated as fuel of solid oxide electrolyte DCFCs (SO-DCFCs). In Zhu's study [11], willow leaves (only baked at 353 K for 1 h and ground into fine powders) was used as fuels of La_{0.75}Sr_{0.25}Cr_{0.5}Mn_{0.5}O_{3-δ} (LSCM) anode SO-DCFC. As the anode chamber was continuously supplied with new willow leaves, peak power density of 330 mW/cm² and duration

over 1000 min without significant performance degradation were obtained at 1073 K. But in more cases, the power densities were lower than 100 mW/cm² and the durability tests were not satisfactory or stable enough to be detected [12-14]. The conversion process and the way to improve the performance have seldom been reported. In addition, the unstable durability has not been studied in detail and the reason of cell degradation is unclear exactly.

For biochar fueled SO-DCFCs, the dominant anode reactions were CO electro-oxidation and C-CO₂ gasification, as suggested by some research groups [15-18]. Anode shielding gas was found to have great impact on the performance of biochar fueled cells, as reported by Dudek et al. [19]. Walnut shells biochar (carbonised at 723 K) produced power density of approximately 119 mW/cm² and 90 mW/cm² at 850 °C when CO₂ and N₂ were used as anode shielding gas respectively. The effect of ash in biochar on the electrochemical performance of SO-DCFC is conflicting. On the one hand, ash species in biochar has been revealed to compromise the stability of SO-DCFC through reducing surface reactive area and blocking charge transfer [13,20,21]. On the other hand, great performance improvement was achieved by introducing common ash species (Ca, Fe, and K et al.) to catalyze the Boudouard reaction [22-25]. It may not be a big issue in DCFCs fueled by low-ash biomass or ash-free carbon materials derived from acid washing and solvent extraction method [26-28]. Although it has been reviewed that elemental composition, particle size, crystallographic disorder, pore size and surface area, surface oxygen functional groups of biochar were critical parameters in determining the polarization performance [9], the optimize of both high and stable power output is still a difficult problem.

Raw biomass, biochar and biogas have been evaluated as fuels in solid oxide fuel cells (SOFCs), but their electrochemical performances have seldom been compared and linked. More importantly, the effect of biomass or biochar fuel property (chemical composition, pyrolysis products, char reactivity, etc.) on the cell performance was not clear exactly. Hence, it is difficult to determine a proper way to convert biomass effectively in solid oxide fuel cells. This study aims to find the relationship of the electrochemical performance between biomass, biochar and biogas in SOFCs, and to reveal the degradation reasons of biomass and biochar fueled cells. The characterization of the thermochemical properties of biomass and biochar, the electrochemical behaviors of biomass, biochar and biogas were studied comprehensively and compared. Then the degradation process of biomass, biochar and biogas fueled SOFCs were analyzed.

2. Material and methods

2.1. Preparation of samples

Two representative biomass wastes, fir sawdust (SD, forest waste) and rice straw (RS, agricultural waste), were used for the experimental materials. As the raw biomass samples both contain considerable oxygen and volatile matter, which was an indicator of low grade energy resource, low temperature thermal pretreatment (torrefaction) and high temperature thermal pretreatment (pyrolysis) were carried out to improve the carbon content. The torrefaction pretreatment was performed under high purity N₂ (99.9%) in a horizontal fixed bed, which was heated from room temperature to 573K and held at 573 K for 30 min. The pyrolysis pretreatment was conducted with the same setup, which was heated from room temperature to 973 K and held at 973 K for 30 min. The pretreated solid products were identified as semi-chars (RS-573 and SD-573) and biochars (RS-973 and SD-973), respectively. The

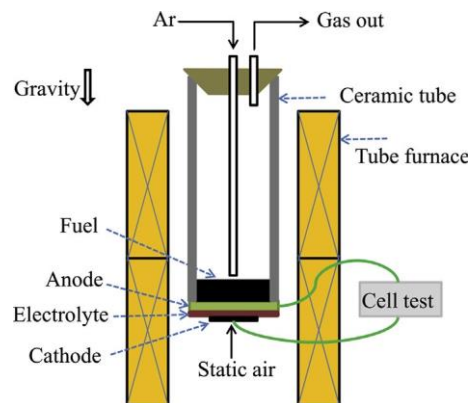


Fig. 1. Electrochemical performance testing system.

Table 1
Proximate and elemental analyses of biomass samples.

Sample	Proximate analysis (wt%, d.b.)			Elemental analysis (wt%, d.a.f.)			
	Volatile matter	Fixed carbon	Ash	C	H	N	O ^a
RS	75.2	15.2	9.6	48.9	5.2	0.9	45.0
RS-573	43.0	35.5	21.5	65.3	5.0	1.3	28.4
RS-973	16.7	48.5	34.8	86.1	2.3	4.8	6.8
SD	85.5	14.1	0.4	50.3	5.9	0.04	43.8
SD-573	67.2	32.0	0.8	62.7	5.5	0.06	31.8
SD-973	17.1	77.2	5.7	90.4	2.4	2.4	4.8

ashes of RS and SD were prepared in a muffle furnace at 673 K.

2.2. Characterization of samples

The proximate analyses and elemental compositions of biomass samples were determined following the Chinese National Standard GB/

^a By difference.

T 28731-2012 and GB/T 31391-2015. The ash samples derived from RS and SD were analyzed via X-ray fluorescence to determine the elemental compositions. The thermal decomposition of raw samples (RS and SD) and semi-chars (RS-573 and SD-573) was performed in a thermogravimetric analyzer (TGA, NETZSCH, STA 449 F3). 5 mg sample was heated from room temperature to 1073 K at a heating rate of 5 K min⁻¹ under N₂ (120 cm³ min⁻¹). The pyrolysis gases were collected in gas bags, and tars were condensed in condenser pipes using liquid nitrogen. The pyrolysis gases were identified by gas chromatograph (Agilent MicroGC 3000). Reactivity of biochar gasification with high purity CO₂ (99.9%) was analyzed in TGA. 5 mg biochar sample was heated from room temperature to 1073 K under N₂ (120 cm³ min⁻¹) at a heating rate of 5 K min⁻¹. Then the temperature was maintained at 1073 K and the purging gas was switched from N₂ to CO₂ (120 cm³ min⁻¹).

2.3. Electrochemical performance evaluation

A schematic diagram of SO-DCFC system employed in this study is shown in Fig. 1. The detailed description of the SO-DCFC system has been introduced elsewhere in the literature [17,29]. The single cell is composed of NiO/Yttria-stabilized zirconia (NiO/YSZ) anode (400 μm), YSZ electrolyte (15 μm), Gd₂O₃-doped CeO₂ (GDC) diffusion barrier layer (2–3 μm) and La_{0.6}Sr_{0.4}Co_{0.2}Fe_{0.8}O_{3-δ} (LSCF)/GDC cathode (25 μm). The anode porosity was 28–32%, estimated by the Archimedes method. The diameter of the anode and cathode is 20 mm and 10 mm, respectively. The active reaction area of the cell is 0.785 cm² (corresponding to the cathode area). Anode shielding gas can be introduced to the anode chamber through a quartz pipe. The cathode was exposed to ambient air. Electrochemical performances, including polarization curves, durability performance and cell resistance were measured by the electrochemical workstation.

For each solid fuel (raw biomass, semi-char and biochar), 0.3 g sample was loaded into anode chamber and in contact with anode

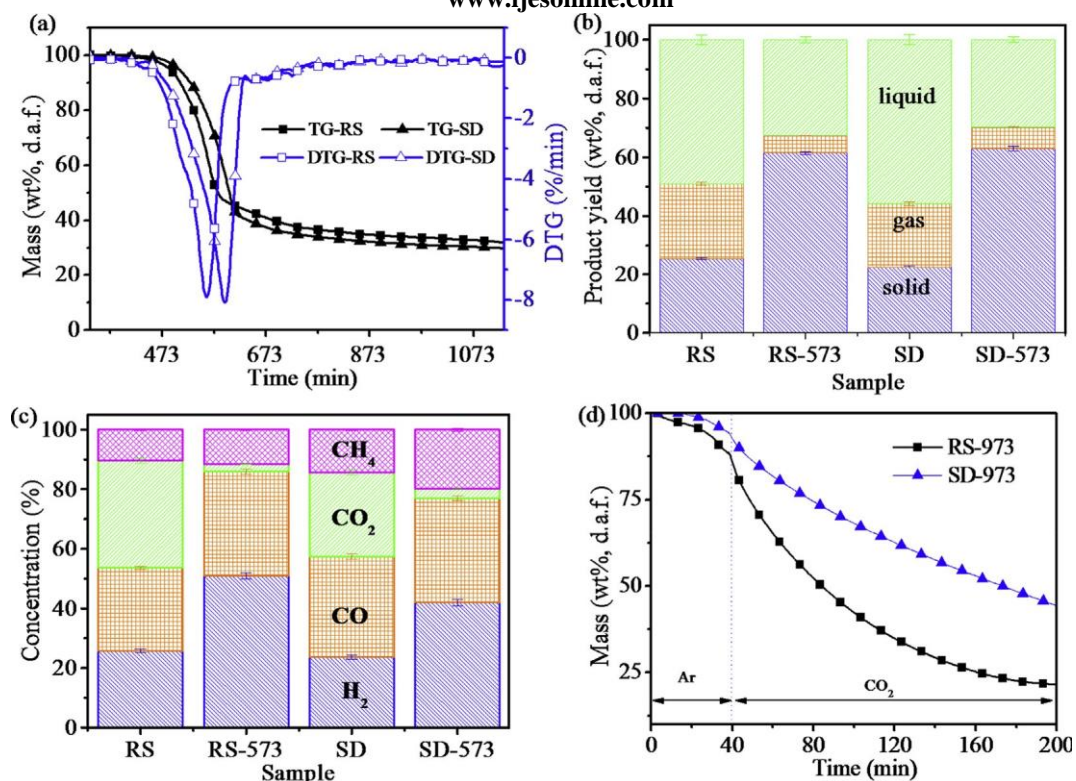


Fig. 2. Pyrolysis and gasification characteristics of samples: (a) weight loss of raw samples during pyrolysis; (b) product yields of raw samples and semi-chars during pyrolysis; (c) gas compositions released by raw samples and semi-chars during pyrolysis; (d) weight loss of biochars during CO₂ gasification process.

surface. The bed height of the samples was around 10 mm in the anode chamber. Prior to heating, 200 cm³ min⁻¹ Ar (high purity, 99.9%) was used to purge the anode chamber for 10 min. Then the furnace was heated from room temperature at a heating rate of 10 K min⁻¹ to 1023 K, 1073 K and 1123 K. Open circuit voltage was monitored during heating process. Each target temperature was maintained for around 5 min to obtain a stable open circuit voltage (OCV) and then the polarization performance was measured. After that, the short-term durability was tested under constant voltage load (0.7 V) at 1123 K. Finally, the cell was cooled down to room temperature with Ar (200 cm³ min⁻¹) purging the anode chamber. The cell anode morphology and elemental information was analyzed using a field emission scanning electron microscopy (SEM) and an X-ray photoelectron spectroscopy (XPS) respectively. XPS measurements were carried out on a ThermoFisher EscaLab 250Xi using a monochromatic Al K α source (E_{photon} = 1486.6 eV). Measurements were carried out in field of 0.5 mm and a pass energy of 30 eV. In order to compensate for the charging of the sample, a charge neutralizer was used.

The electrochemical characteristics of biochar under different atmosphere were also investigated in SO-DCFCs at 1023–1123 K. The polarization performance of biochar fueled cells under None/Ar/CO₂ atmosphere and varying CO₂ flow rate (0–200 cm³ min⁻¹) was tested by switching anode purging gas and adjusting CO₂ flow rate. In the same fuel cell system, the electrochemical behavior of pyrolysis gas products was investigated by continuously feeding simulated biogas into the anode chamber instead of solid carbon. The biogas was prepared based on the pyrolysis gas compositions of RS and SD. The cell was heated to 973 K under 200 cm³ min⁻¹ H₂ (20 vol%, Ar as the balance gas) to reduce the anode. The polarization curve of H₂ was tested

for the benchmark purpose. Then the anode gas was switched to Ar for 10 min to drive away the residual H₂ in the anode. After that, the anode gas was switched to biogas (5–80 cm³ min⁻¹). The electrochemical performance measurement process was the same as that of solid carbon fuels.

3. Results and discussion

3.1. Thermochemical properties of biomass samples

The proximate and elemental analyses of samples are shown in [Table 1](#). It can be found that both rice straw (RS) and fir sawdust (SD) contain high content of volatile matter, 75.2% and 85.5% respectively. Thermal pretreatment at 573 and 973 K resulted in the dramatically decrease of volatile and oxygen content, and the increase of fixed carbon and ash content. For the chars, the content of volatile matter declined to around 17%, and the fixed carbon content of RS-973 and SD-973 increased to 48.5% and 75.2%. RS-973 has high ash content of 34.8%, as the pyrolysis resulted in the enrichment of mineral species in the biochar.

The thermal decomposition behaviors of RS and SD are shown in [Fig. 2a](#), which reveals that most of the volatiles were released before 673 K. It was in good consistence with the proximate analysis that semi- chars (RS-573 and SD-573) still contained considerable volatile matter. The yield distribution of raw samples and semi- chars during pyrolysis process at 973 K is shown in [Fig. 2b](#). For the raw samples, the yields of

solid, gas and liquid products were around 22–26%, 21–26% and 48–57% respectively. For semi- chars, the solid char yield increased to 61.4% (RS-573) and 62.9% (SD-573). Accordingly, the liquid tar yield

decreased to 32.7% (RS) and 29.8% (SD). More significant decrease of the gas product yield can be observed for both RS-573 (5.9%) and SD- 573 (7.3%). It was suggested that torrefaction pretreatment was an effective method to suppress tar/gas formation during biomass pyrolysis. As shown in [Fig. 2c](#), the concentrations of pyrolysis gases for raw samples (RS and SD) were similar, around 25% H₂, 30% CO, 32% CO₂ and 13% CH₄. For semi- chars (RS-573 and SD-573), the concentrations of H₂ and CH₄ in pyrolysis gases increased, while the concentration of CO₂ decreased because of the reduced oxygen-containing functional groups. [Fig. 2d](#) compares the weight loss curves of SD-973 and RS-973 during gasification process. Clearly, the gasification reactivity of RS-

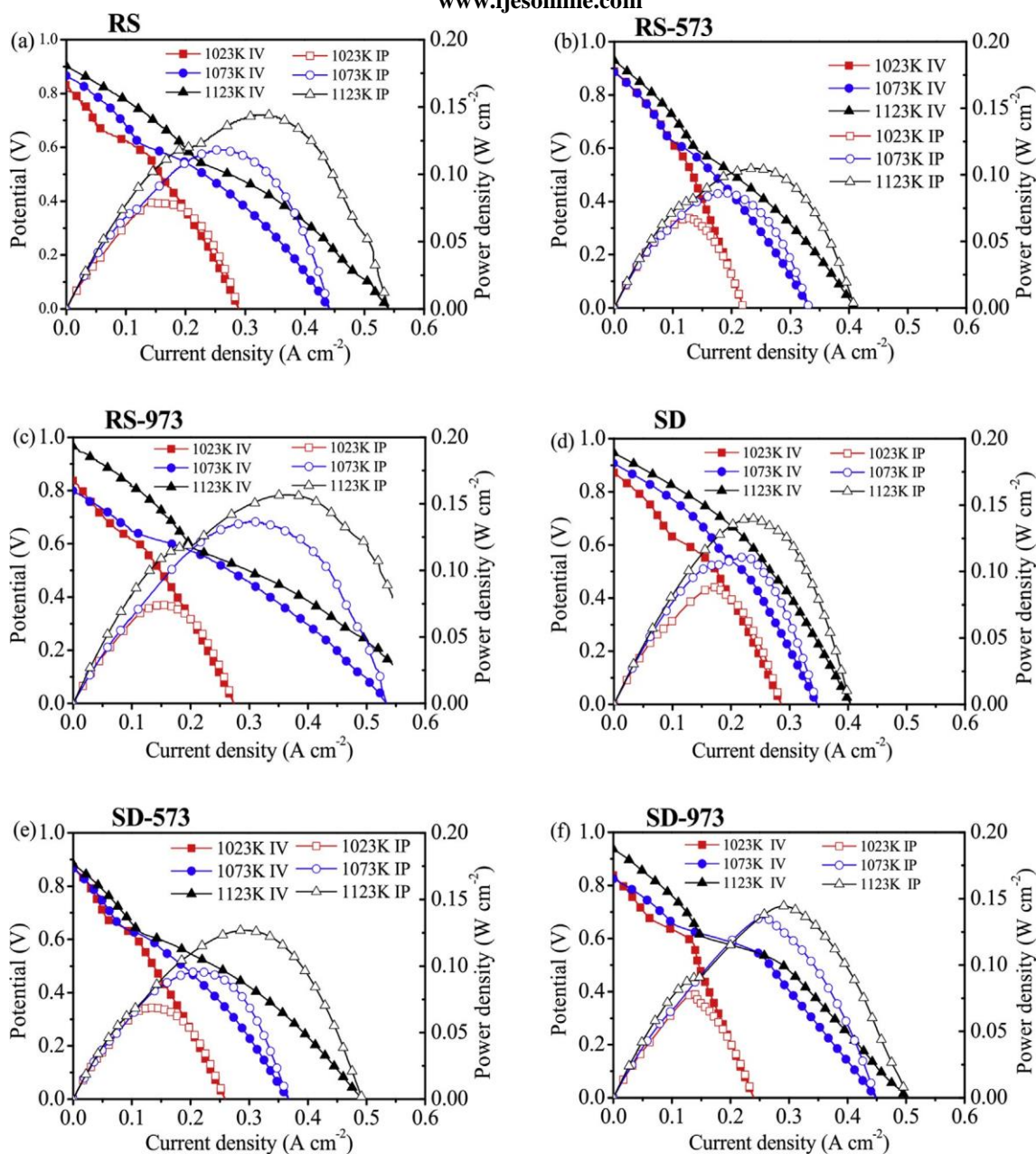


Fig. 3. Current density-Potential and Current density-Power density curves of (a) RS, (b) RS-573, (c) RS-973, (d) SD, (e) SD -573, (f) SD-973.

Table 2
 PPDs and OCVs of raw, torrefacted and pyrolyzed samples.

Fuel	PPD ($W\ cm^{-2}$)			OCV (V)		
	1023K	1073K	1123K	1023K	1073K	1123K
RS	0.080	0.118	0.144	0.84	0.86	0.91
RS-573	0.067	0.086	0.105	0.88	0.88	0.92
RS-973	0.074	0.137	0.157	0.83	0.81	0.98
SD	0.088	0.111	0.140	0.88	0.91	0.95
SD-573	0.068	0.096	0.127	0.87	0.88	0.88
SD-973	0.079	0.136	0.145	0.83	0.82	0.94
Biogas	0.120	0.132	0.139	1.05	1.04	1.04

973 was much higher than that of SD-973, which may be attributed to its higher mineral content (Table 1). Mineral components such as K, Ca and Fe species in RS ash (Supplementary material, Table S1) is widely accepted as good catalyst for char-CO₂ gasification.

3.2. Electrochemical performance of raw, torrefacted and pyrolyzed samples

The polarization curves of raw samples, semi-chars and biochars are shown in Fig. 3. The peak power densities (PPDs), OCVs extracted from the polarization curves are shown in Table 2. It's quite clear that the PPDs, OCVs and maximum current densities (MCDs) of all the samples increased remarkably with cell temperature rising from 1023 to 1123 K. Taking SD for example, the OCVs, MCDs and PPDs increased from 0.88 V, 0.28 A cm⁻² and 0.088 W cm⁻² at 1023 K to 0.95 V, 0.48 A cm⁻² and 0.140 W cm⁻² at 1123 K respectively. The polarization characteristics of RS were similar with that of SD, which were greatly dependent on the cell temperature. In the same SOFC system, 20 vol% H₂ was used as anode fuel for benchmark purpose. The electrochemical performance of raw biomass was considerable compared with the PPD of 20 vol% H₂ (0.092 W cm⁻², 1023 K). The semi-chars, RS-573 and SD-573, both delivered lower PPDs than the raw samples. For RS-973 and SD-973, the PPDs were more sensitive to the

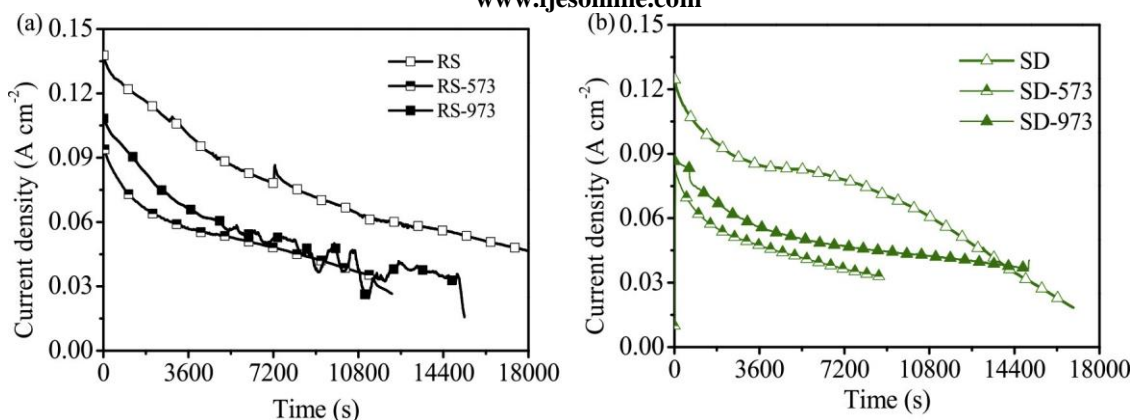


Fig. 4. Short-term durability of raw samples, semi-chars and biochars.

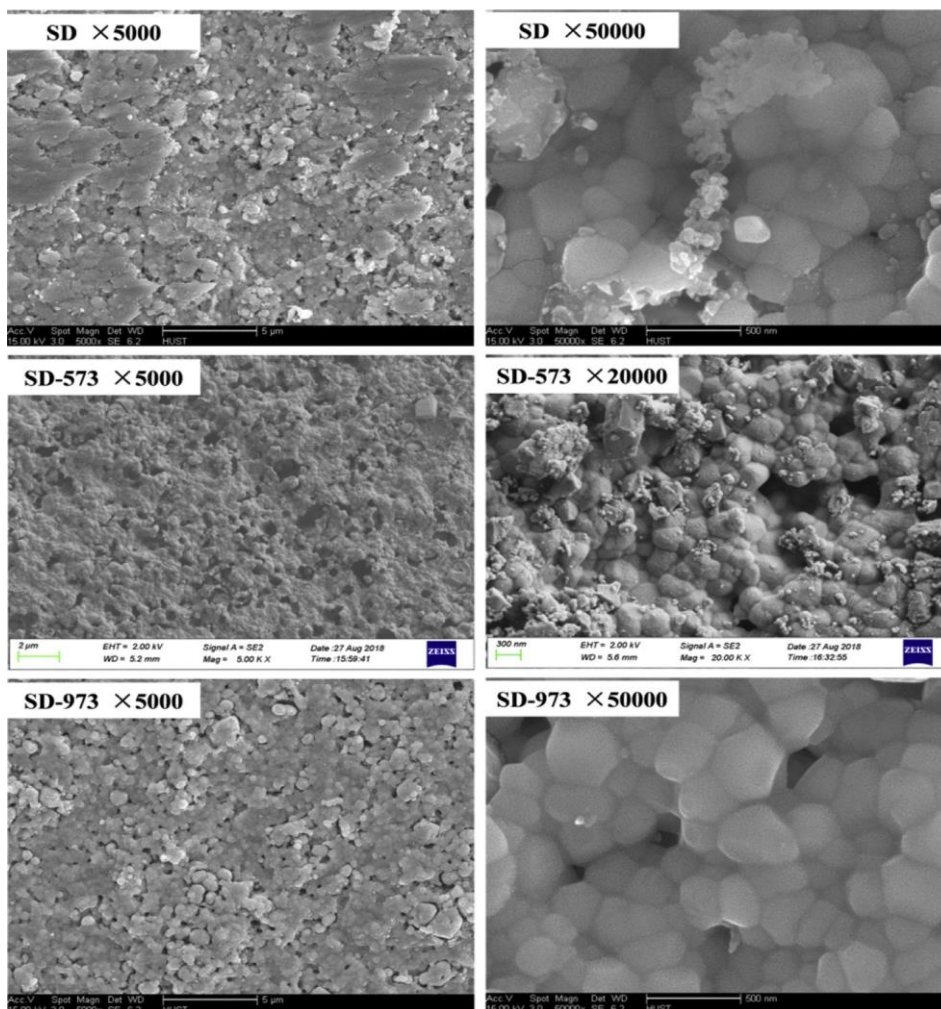


Fig. 5. Anode morphologies after durability tests: (a) SD, magnified 5000 times; (b) SD, magnified 50000 times; (c) SD-573, magnified 5000 times; (d) SD-573, magnified 20000 times; (e) SD, magnified 5000 times; (f) SD-973, magnified 50000 times.

temperature variation. At 1023 K, the PPDs and OCVs were slightly lower than that of the raw samples. As the cell temperature rose to 1073 and 1123 K, the PPDs and OCVs became even higher than that of the raw samples.

The short-term durability tests of the sample are shown in Fig. 4. It can be seen that all the fuels generated unstable current density under constant voltage load of 0.7 V. For the raw samples, the initial current density was much higher than that of semi-chars and biochars. But also,

Table 3
XPS elemental analysis results for different anode surfaces.

Elements	Atomic percentage (at %)				
	SD	SD-573	SD-973	biogas	blank
C	26.15	18.29	22.26	36.85	6.12
O	52.45	48.18	55.24	45.96	56.08
Ni	6.72	28.23	6.06	1.94	15.24
Y	2.01	0.76	2.22	2.03	1.96
Zr	12.66	4.54	14.21	13.22	20.61

it was shown that the current density of the raw samples generally dropped faster than that of semi-chars and biochars. The current density of SD was even lower than that of SD-973 after 14400 s. Compared with biochars, semi-chars displayed lower current output and more rapid current decline for both RS and SD. The current density of RS-973 fluctuated widely after 7200 s discharge, which was more unstable than that of SD-973. The anode morphologies after durability tests of SD, SD-573 and SD-973 are shown in Fig. 5. As a reference, the anode porous morphology of the blank cell was provided in our previous study [17], which possessed porous and homogeneous structure. With SD as fuel, it can be observed that the anode surface was covered by some bulk in the view of 5000 times, resulting in that the anode pores presented inhomogeneous distribution on the surface. SEM image of 50000 times confirmed the existence of clusters of carbon deposits. With SD-573 as fuel, the anode surface was also uniform with considerable carbon deposits on the anode surface. The anode surface of SD-973 fueled cell was much cleaner than that of SD and SD-573 in images of both 5000 and 50000 times. However, its surface morphology is not uniform enough compared with that of the blank cell. According to the anode morphologies, it can be deduced that the carbon deposits of SD were worse than that of SD-573 and SD-973. The carbon deposits blocked the anode pores and increased the transfer resistance of active species to

the anode reactive sites, leading to current degradation.

XPS was used to further characterize the anodic carbon deposition on the anode surfaces after the tests. Table 3 shows the atomic percentages of Ni, Y, Zr, C and O in the anode surfaces for different fuels. The blank cell, which was reduced by H₂ at 973 K for 3 h, was measured for bench mark purpose. The XPS analysis results for the blank cell indicate a little carbon (6.12%) in the anode after the H₂ reduction even without biomass fuels, which was probably introduced by the carbon-containing pore former in the cell fabrication process [30]. For SD, SD-573 and SD-973 fueled cells, considerable carbon deposition was detected on each anode surface. Especially, the carbon percentage of SD fueled cell was as high as 26.15%, which was consistent with the anode morphologies. Although no obvious carbon deposit was observed on the anode morphology of SD-973 fueled cell, there was still 22.26% carbon detected by XPS analysis.

Deposited carbon on the anode via thermal pyrolysis of hydrocarbon gases has been demonstrated to be used as anode fuel and participate in anode electrochemical reactions in Ni/YSZ and Ni/GDC anode [31,32]. However, the location and size of the carbon deposit on the anode are important considerations. It was revealed that carbon deposit could be formed on the Ni surface, the YSZ particle surface and at the three-phase boundary (TPB), however electrochemical reactions of the deposited carbon are most difficult on the Ni particle surfaces, easier on the YSZ particle surfaces and easiest at the TPB. Not all of the deposited carbon participated in the direct electrochemical reactions [33]. In the present study, the C1s XPS peak was deconvoluted into four peaks (Fig. 6) corresponding to graphitic carbon (GC) (284.6 eV), carbon in single C-O bonds as ethers, alcohols, and phenols (286.3 eV), carbon in carbonyl groups (C=O) (287.4 eV), carbon in carboxyl or ester groups (O-C=O) (288.8 eV) [34-36]. Accordingly, the relative atomic percentages of carbon-based functional groups are shown in Table 4. The results showed that carbon deposits mainly existed in the form of GC, C-O and O-C=O groups on the anodes with SD, SD-573

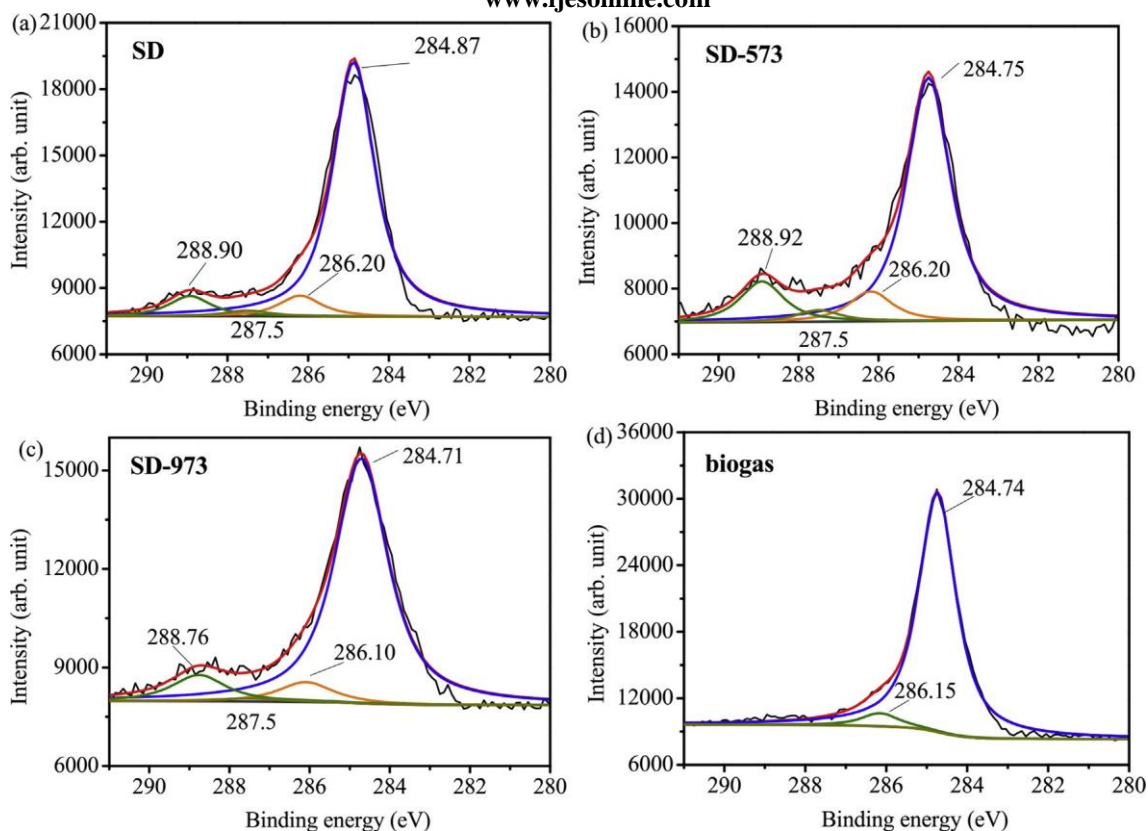


Fig. 6. Deconvolution of C1s XPS spectra: (a) SD, (b) SD-573, (c) SD-973 and (d) biogas.

Table 4
 Deconvolution results of the C 1s XPS spectra.

Cases	C 1s deconvolution results				
	Formation	Binding energy (eV)	Half peak width (eV)	Area	Percentage (%)
SD	GC (284.6eV)	284.87	1.236	20950.8	84.64
	C-O (286.3eV)	286.20	1.236	1699.8	6.87
	C=O (287.4eV)	287.50	1.236	448.4	1.81
	O-C-O (288.8eV)	288.90	1.236	1654.8	6.68
SD-573	GC (284.6eV)	284.75	1.296	14153.6	74.82
	C-O (286.3eV)	286.20	1.296	1734.0	9.17
	C=O (287.4eV)	287.50	1.296	674.3	3.56
	O-C-O (288.8eV)	288.92	1.296	2355.4	12.45
SD-973	GC (284.6eV)	284.71	1.592	17458.1	83.23
	C-O (286.3eV)	286.10	1.592	1416.8	6.75
	C=O (287.4eV)	287.50	1.592	226.0	1.08
	O-C-O (288.8eV)	288.70	1.592	1874.8	8.94
biogas	GC (284.6eV)	284.74	1.099	34912.8	94.62
	C-O (286.3eV)	286.15	1.099	1886.2	5.11
	C=O (287.4eV)	287.40	1.099	97.7	0.26

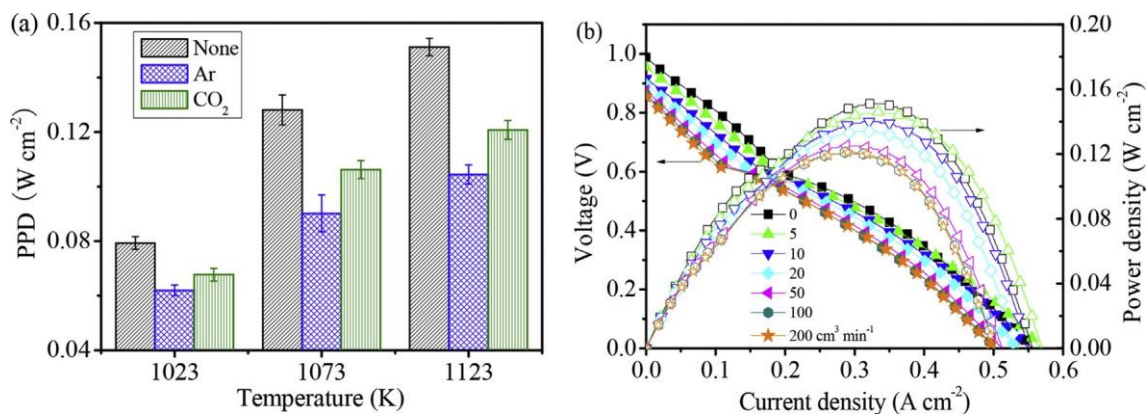


Fig. 7. Electrochemical performance of RS-973 fueled cell: (a) under None/Ar/CO₂ atmosphere; (b) under varying flow rate of CO₂.

and SD-973 as fuels. C-O groups could be ignored because of its much lower percentage (<4%) in all cases. Compared with C-O, C-O and O-C-O, the content of GC was much higher, ranging from 74.82% ~94.62%. These graphitic carbon deposits were more difficult to be consumed by direct electrochemical reaction or in-situ gasification than to carbon atoms bound to oxygen (C-O, C-O and O-C-O).

It is worth noting that the two raw biomass materials have similar polarization performance; the semi-chars, and bio-chars from the two biomasses also have the similar polarization output, respectively (Fig. 3, Table 2). However, the durability tests (Fig. 4) show some different behaviors between the pairs. Generally, the polarization performance is an initial and transient electrochemical parameter to evaluate the electrochemical reactivity of anode fuels. On the contrary, the durability performance is a long-term stability behavior, and is related to not only the initial fuel reactivity but also the fuel evolution and their impact on the anode activity during discharge process. For raw biomass pairs or semi-char pairs, their polarization performance was largely controlled by their pyrolysis gas compositions. As shown in Fig. 2c, the concentrations of the active gases, especially H₂, between the pairs were similar, predicting the similarity of the polarization performance between the raw biomass pairs or semi-char pairs. During the durability test of raw biomass pairs and semi-char pairs, carbon deposit was formed by the cracking of CO and CH₄ or some other heavy hydrocarbon (liquid products), causing rapid cell degradation. The

durability of SD was more unsteady than that of RS due to its higher concentration of CO and CH₄ and higher yield of liquid hydrocarbons in the pyrolysis products. For the bio-char pairs, they displayed similar initial discharge current density, which was in consistent with their

polarization performance at 1123 K. After that, RS-973 showed more unstable discharge process than SD-973. It may be attributed to the much higher ash content in RS-973 than SD-973. The negative effects of traditional ash species on the Ni/YSZ anode SOFC have been revealed in our previous study [20].

3.3. Electrochemical performance of biochar and biogas

To figure out the degradation of biomass fueled cells, the electro-chemical performances of biochar under different anode atmosphere and biogas were evaluated. First, the polarization performance of RS-973 under different atmosphere was tested and the PPDs are extracted as shown in Fig. 7a. Clearly, both the temperature and anode atmosphere had significant influence on the cell performance. Raising the temperature from 1023 to 1123K helped to drastically improve the PPDs due to reduced anode ohmic resistance and enhanced fuel mass transfer. Comparing the PPDs under these 3 atm, it was obvious that the PPDs were the highest with none gas purging and the lowest with inert gas (Ar , $200 \text{ cm}^3 \text{ min}^{-1}$) purging at 1023–1123 K. It has been demonstrated by our previous study and others' that the dominant anode reactions of Ni/YSZ anode supported SO-DCFC were CO electro-oxidation (Reaction 1) and C-CO₂ gasification (Reaction 2) [15–18]. It's easy to understand that continuous Ar feeding diluted the anode active reactant and caused the decrease of available CO around the anode active sites. It was worth noting that continuous CO₂ feeding ($200 \text{ cm}^3 \text{ min}^{-1}$) did not contribute to higher performance than none gas feeding. CO₂ can on one hand improve gasification rate of char, and on the other hand act as diluent. The improved gasification may contribute higher CO supply,

7

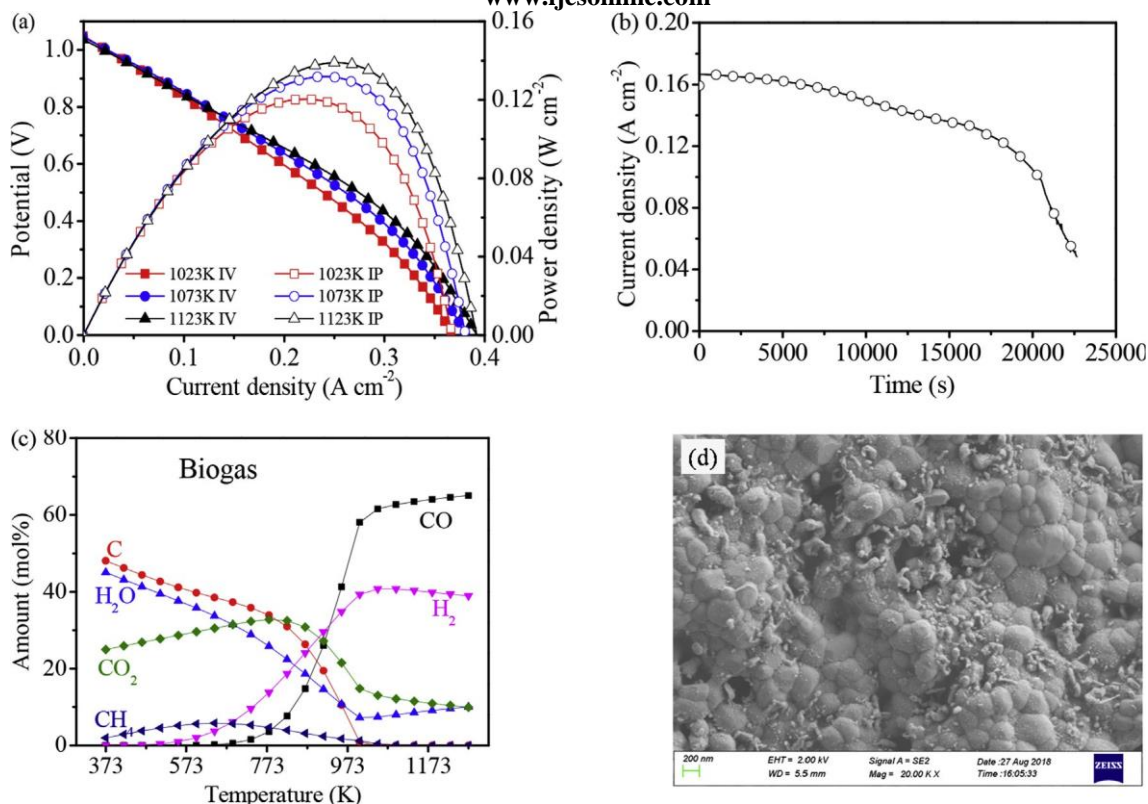


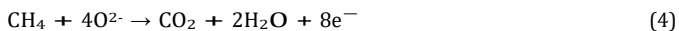
Fig. 8. Electrochemical performance of biogas fueled cell: (a) polarization performance; (b) durability performance; (c) thermodynamic equilibrium compositions of biogas; (d) anode surface morphology.

while the dilution effect may lower CO concentration near the anode surface. The joint effect may be closely related to the CO₂ feeding rate, as the amount of CO consumed during polarization test was much less than that produced by char-CO₂ gasification. The polarization performance of under varying CO₂ flow rate was tested, as shown in Fig. 7b. It showed that gradual increase of CO₂ flow rate from 0 to 200 cm³ min⁻¹ resulted in lower cell polarization performance. Based the measured performance, it can be concluded that CO₂ feeding resulted in the decrease of available CO concentration near the anode active sites. Accelerating Char-CO₂ gasification rate by introducing CO₂ did not contribute to higher polarization performance but dilute active gas.

Anode reactions of biochar fueled cell:



Anode reactions of biogas fueled cell:



As indicated by the pyrolysis characteristics of raw samples (Fig. 2), the gas products accounted for 20–25% yield and mainly consisted of H₂, CO, CO₂ and CH₄, suggesting that their electrochemical contribution in SO-DCFC should not be ignored. According to the pyrolysis gas compositions derived from RS and SD, gas mixture (named as biogas, composed of 24.46% H₂, 30.98% CO, 32.53% CO₂ and 12.03% CH₄) was prepared and used to simulate the actual pyrolysis gas products. The electrochemical performance of biogas fueled SOFC is shown in

electrochemical oxidation of the active species in biogas (Reaction 1, 3, 4) contributed greatly to the cell polarization performance. At 1123 K, the PPD increased to 0.139 W cm⁻², which was lower than that of raw samples at 1123 K. The discharge current density of biogas was higher and more stable than that of solid fuels in the first 20000 s, but dropped sharply at around 20000 s (Fig. 8b). Although negligible amounts of carbon deposits were predicted at 1023–1123 K by thermodynamic equilibrium analysis (Fig. 8c) using HSC chemistry (Version 6.0, Outokumpu Research Oy, Finland), severe carbon deposits were still formed in biogas fueled cell anode (as shown in Figs. 8d and 6d and Table 4) and caused cell degradation. Furthermore, it's also indicated by the XPS analysis (Table 4) that the anode carbon deposits of both biochar and biogas fueled fuels were largely in the form of graphitic carbon. Besides, it can be also found in Table 4 that graphitic carbon Fig. 8. The corresponding PPDs and OCVs were listed in Table 2. It can be found in Fig. 8a that excellent polarization performance was acquired by feeding biogas into the anode. At 1023 K, the PPD and OCV were 0.120 W cm⁻² and 1.05 V, much higher than that of the solid fuels and 20 vol% H₂ (0.092 W cm⁻²), demonstrating that the

dominated deposits on the anode surface for all the fuels. The mechanism of carbon deposit formation on porous metal materials has been described in detail in Ref. [37]. It was revealed that temperature was a key factor to determine the form of the carbon deposit. With the temperature increasing, the more reactive and amorphous forms of carbon deposits forming at low temperatures tended to convert to the less reactive and graphitic forms. In the present study, although the anode gas composition showed some difference with these fuels (raw biomass, semi-chars, biochars, and biogas) feeding the anode, the cell temperature all ranged from 750 to 850 °C, which was more beneficial for the formation of graphitic carbon.

Based on the discussion above, it can be concluded that raw biomass, biochar and biogas all had the capability of generating electricity in SOFCs. For raw biomass, its electrochemical performance was the combined electrochemical result of biochar and biogas. Both biogas (containing H₂, CO, CH₄, etc.) and biochar generated considerable power density at 1023–1123 K, and their anode reactions and degradation mechanisms were different. The electrochemical reactions of biogas fueled cell included the electro-oxidation of CO, H₂, CH₄ and

maybe some other light hydrocarbons. The cell degradation was mainly caused by severe anode graphitic carbon deposition, which blocked the anode pores and increased the mass transfer resistance of active species into the anode TPB sites, and even worse, migrated onto the nickel bulk and caused irreversible anode deterioration. For biochar fueled cell, the anode reactions were mainly CO electro-oxidation and char-CO₂ gasification. Anode shielding gas showed significant impact in the cell performance and continuously feeding of CO₂ to the anode chamber did not improve the power output. The cell degradation was due to slight carbon deposition and the decreasing reactivity of char gasification with CO₂.

4. Conclusions

In this study, the electrochemical performance and degradation behaviors of two traditional biomass wastes and their decomposition products were evaluated in SOFCs. The relationship of electrochemical performance between biomass and its decomposition products was clarified. The direct utilization of biomass in SOFC produced considerable power output (~0.140 W cm⁻² at 1123 K) but cannot maintain stable discharge. Torrefaction (573 K) pretreatment of raw samples compromised peak power densities (PPDs), while pyrolysis (973 K) pretreatment enhanced PPDs at 1073 and 1123 K. Cells fueled by biomass, biochar and biogas all suffered from anode carbon deposits, most of which were in the form of graphitic carbon. When raw biomass was used as fuel directly, its thermal decomposition products, both biochar and biogas, were involved in anode electrochemical reactions, generating comparable power densities and also contributing greatly to the cell degradation. With biochar as fuel, the dominant anode reactions were CO electro-oxidation and biochar-CO₂ gasification. Continuously feeding of CO₂ to the anode chamber did not improve the output performance. The discharge degradation was mainly caused by the gradually decreasing gasification reactivity of biochar with CO₂ and slight anode carbon deposition. With biogas as fuel, the anode reactions were the electro-oxidation of CO, H₂, CH₄ and maybe some other light hydrocarbons. The cell degraded due to severe anode carbon deposition. The electrochemical output and degradation behavior of raw biomass were determined by the electrochemical contribution of its thermal decomposition products.

References

- [1] T.M. Gür, Critical review of carbon conversion in "carbon fuel cells", *Chem. Rev.* 113 (2013) 6179–6206.
- [2] S. Giddey, S.P.S. Badwal, A. Kulkarni, C. Munnings, A comprehensive review of direct carbon fuel cell technology, *Prog. Energ. Combust.* 38 (2012) 360–399.
- [3] D. Cao, Y. Sun, G. Wang, Direct carbon fuel cell: fundamentals and recent developments, *J. Power Sources* 167 (2007) 250–257.
- [4] C. Jiang, J. Ma, G. Corre, S.L. Jain, J. Irvine, Challenges in developing direct carbon fuel cells, *Chem. Soc. Rev.* 46 (2017) 2889–2912.
- [5] A.C. Rady, S. Giddey, S.P.S. Badwal, B.P. Ladewig, S. Bhattacharya, Review of fuels for direct carbon fuel cells, *Energy Fuel* 26 (2012) 1471–1488.
- [6] Y. Chen, X. Zhang, W. Chen, H. Yang, H. Chen, The structure evolution of biochar from biomass pyrolysis and its correlation with gas pollutant adsorption performance, *Bioresour. Technol.* 246 (2017) 101–109.
- [7] H. Hassan, J.K. Lim, B.H. Hameed, Recent progress on biomass co-pyrolysis conversion into high-quality bio-oil, *Bioresour. Technol.* 221 (2016) 645–655.
- [8] M. Sharma, R. N. S. Dasappa, Solid oxide fuel cell operating with biomass derived producer gas: status and challenges, *Renew. Sustain. Energy Rev.* 60 (2016) 450–463.
- [9] N. Jafri, W.Y. Wong, V. Doshi, L.W. Yoon, K.H. Cheah, A review on production and characterization of biochars for application in direct carbon fuel cells, *Process Saf. Environ.* 118 (2018) 152–166.
- [10] S.A. Saadabadi, A. Thallam Thattai, L. Fan, R.E.F. Lindeboom, H. Spanjers, P.V. Aravind, Solid oxide fuel cells fuelled with biogas: potential and constraints, *Renew. Energy* 134 (2019) 194–214.
- [11] X. Zhu, Y. Li, Z. Lü, Continuous conversion of biomass wastes in a La_{0.75}Sr_{0.25}Cr_{0.5}Mn_{0.5}O_{3-δ} based carbon–air battery, *Int. J. Hydrogen Energy* 41 (2016) 5057–5062.
- [12] B.R. Alexander, R. Mitchell, T.M. Gür, Biomass conversion in a solid oxide fuel cell, *Ecs Transactions* 35 (2011) 2685–2692.
- [13] C. Munnings, A. Kulkarni, S. Giddey, S.P.S. Badwal, Biomass to power conversion in a direct carbon fuel cell, *Int. J. Hydrogen Energy* 39 (2014) 12377–12385.
- [14] A.C. Lee, S. Li, R.E. Mitchell, T.M. Gür, Conversion of solid carbonaceous fuels in a fluidized bed fuel cell, *Electrochem. Solid State Lett.* 11 (2008) B20–B23.
- [15] Y. Xie, Y. Tang, J. Liu, A verification of the reaction mechanism of direct carbon solid oxide fuel cells, *J. Solid State Electrochem.* 17 (2013) 121–127.
- [16] T.M. Gür, Mechanistic modes for solid carbon conversion in high temperature fuel cells, *J. Electrochem. Soc.* 157 (2010) B751–B759.
- [17] K. Xu, H. Hu, Z. Li, X. Zhu, H. Liu, G. Luo, X. Li, H. Yao, Investigation of the anode reactions in solid oxide electrolyte based carbon fuel cells, *Int. J. Hydrogen Energy* 42 (2017) 10264–10274.
- [18] Y. Tang, J. Liu, Effect of anode and Boudouard reaction catalysts on the performance of direct carbon solid oxide fuel cells, *Int. J. Hydrogen Energy* 35 (2010) 11188–11193.
- [19] M. Dudek, B. Adamczyk, M. Sitarz, M. Śliwa, R. Lach, M. Skrzyplikiewicz, A. Raźniak, M. Ziąbka, J. Zupała, P. Grzywacz, The usefulness of walnut shells as waste biomass fuels in direct carbon solid oxide fuel cells, *Biomass Bioenergy* 119 (2018) 144–154.
- [20] K. Xu, J. Dong, H. Hu, X. Zhu, H. Yao, Effect of ash components on the performance of solid oxide electrolyte-based carbon fuel cells, *Energy Fuel* 32 (2018) 4538–4546.
- [21] G. Liu, A. Zhou, J. Qiu, Y. Zhang, J. Cai, Y. Dang, Utilization of bituminous coal in a direct carbon fuel cell, *Int. J. Hydrogen Energy* 41 (2016) 8576–8582.
- [22] X. Yu, Y. Shi, H. Wang, N. Cai, C. Li, A.F. Ghoniem, Using potassium catalytic gasification to improve the performance of solid oxide direct carbon fuel cells: experimental characterization and elementary reaction modeling, *J. Power Sources* 252 (2014) 130–137.
- [23] A.C. Rady, S. Giddey, A. Kulkarni, S.P.S. Badwal, S. Bhattacharya, Catalytic gasification of carbon in a direct carbon fuel cell, *Fuel* 180 (2016) 270–277.
- [24] W. Cai, Q. Zhou, Y. Xie, J. Liu, A facile method of preparing Fe-loaded activated carbon fuel for direct carbon solid oxide fuel cells, *Fuel* 159 (2015) 887–893.
- [25] Q. Qiu, M. Zhou, W. Cai, Q. Zhou, Y. Zhang, W. Wang, M. Liu, J. Liu, A comparative investigation on direct carbon solid oxide fuel cells operated with fuels of biochar derived from wheat straw, corncob, and bagasse, *Biomass Bioenergy* 121 (2019) 56–63.
- [26] H. Ju, J. Eom, J.K. Lee, H. Choi, T. Lim, R. Song, J. Lee, Durable power performance of a direct ash-free coal fuel cell, *Electrochim. Acta* 115 (2014) 511–517.
- [27] M. Dudek, P. Tomczyk, R. Socha, M. Hamaguchi, Use of ash-free "Hyper-coal" as a fuel for a direct carbon fuel cell with solid oxide electrolyte, *Int. J. Hydrogen Energy* 39 (2014) 12386–12394.
- [28] M. Dudek, M. Skrzyplikiewicz, N. Moskała, P. Grzywacz, M. Sitarz, I. Lubarska-Radziejewska, The impact of physicochemical properties of coal on direct carbon solid oxide fuel cells, *Int. J. Hydrogen Energy* 41 (2016) 18872–18883.
- [29] K. Xu, Z. Li, M. Shi, H. Xing, H. Liu, X. Li, H. Hu, G. Luo, H. Yao, Investigation of the anode reactions in SO-DCFCs fueled by Sn-C mixture fuels, *Proc. Combust. Inst.* 36 (2017) 4435–4442.
- [30] C. Li, Y. Shi, N. Cai, Carbon deposition on nickel cermet anodes of solid oxide fuel cells operating on carbon monoxide fuel, *J. Power Sources* 225 (2013) 1–8.
- [31] M. Ihara, S. Hasegawa, Quickly rechargeable direct carbon solid oxide fuel cell with propane for recharging, *J. Electrochem. Soc.* 153 (2006) A1544–A1546.
- [32] S. Hasegawa, M. Ihara, Reaction mechanism of solid carbon fuel in rechargeable direct carbon SOFCs with methane for charging, *J. Electrochem. Soc.* 155 (2008) B58–B63.
- [33] C. Li, Y. Shi, N. Cai, Mechanism for carbon direct electrochemical reactions in a solid oxide electrolyte direct carbon fuel cell, *J. Power Sources* 196 (2011) 754–763.
- [34] A.B. Dongil, B. Bachiller-Baeza, A. Guerrero-Ruiz, I. Rodríguez-Ramos, A. Martínez-Alonso, J.M.D. Tascón, Surface chemical modifications induced on high surface area graphite and carbon nanofibers using different oxidation and functionalization treatments, *J. Colloid Interface Sci.* 355 (2011) 179–189.

- [35] H. Estrade-Szwarckopf, XPS photoemission in carbonaceous materials: a "defect" peak beside the graphitic asymmetric peak, *Carbon* 42 (2004) 1713–1721.
- [36] B. Jarrais, A. Guedes, C. Freire, Selectively oxidized carbon nanocatalysts for the oxidation of cis-cyclooctene, *New J. Chem.* 42 (2018) 2306–2319.
- [37] C.H. Bartholomew, Carbon deposition in steam reforming and methanation, *Catal.Rev.* 24 (1982) 67–112.